ISSN: 2395-1680 (ONLINE)
DOI: 10.21917/ijme.2018.0103

MATHEMATICAL MORPHOLOGY BASED FAULT DETECTOR FOR PROTECTION OF DOUBLE CIRCUIT TRANSMISSION LINE

Gaurav Kapoor
Department of Electrical Engineering, Modi Institute of Technology, India
E-mail: gaurav.kapoor019@gmail.com

Abstract

This paper presents mathematical morphology based fault detector for the protection of double circuit transmission line. Three phase fault current of both circuits measured at relay location is processed using mathematical morphology. Performance of the proposed fault detector is tested for different types of shunt faults. The simulation results demonstrate that the proposed mathematical morphology based fault detector accurately detects the fault and identifies the faulty phase of a double circuit transmission line and is not affected by variation in fault parameters.

Keywords:

Mathematical Morphology, Fault Detection and Double Circuit Transmission Line Protection

1. INTRODUCTION

To sustain consistent supply of electrical power, modern extra high voltage double circuit transmission lines necessitate faults to be detected and located quickly. Detection of fault in double circuit transmission line is a very convoluted task due to a serious problem of mutual coupling between the phases of two circuits. For the protection of double circuit transmission line, various researchers proposed their schemes to detect and locate faults. Along with the various schemes introduced so far, differential power approach was used by the researchers for the protection of double circuit transmission line in [1]. For the protection of parallel transmission lines, researchers in [2] used the approach of Naïve Bayes classifier. Fault location technique using distributed parameter line model for series compensated double circuit transmission line protection was introduced in [3]. In [4], a combined scheme based on discrete wavelet transform and artificial neural network for parallel transmission line protection had been illustrated. Artificial neural network had been used for detection and classification of transmission line faults in [5]. For the protection of series compensated transmission line, a backup distance protection scheme was introduced in [6]. In [7], a high-speed scheme of finding out faulted circuit of parallel transmission line using single end measurement was introduced. A protection scheme for series compensated double circuit transmission line which uses the direction of current transients was proposed in [8]. For the protection of first zone of series compensated double circuit transmission line, a digital relaying scheme was introduced in [9]. A relaying scheme based on adaptive cumulative sum was used in [10], for the protection of double circuit transmission line. Artificial neural network had been used for the detection and classification of six phase transmission line faults [11]. A technique for the location of faults and selection of faulty phase in six phase transmission line was described in [12]. Voltage stability analysis of six phase transmission line had been done by the researchers in [13]. Artificial neural network was used for the protection of series compensated transmission lines in [14]. Wavelet transform was used for the protection of series compensated transmission line [15].

In the present work, mathematical morphology approach for the detection of fault and identification of faulty phase is presented. The performance of proposed technique has been tested for different types of shunt faults. Simulation results of mathematical morphology, on a double circuit transmission line test system for various types of fault conditions, indicates that the proposed fault detector accurately detects the fault and identifies the faulty phase.

This paper is organized as follows: section 2 of the paper is devoted to the simulation study of double circuit transmission line using MATLAB software. Section 3 gives an introduction on mathematical morphology and its application to transmission line protection. Section 4 introduces mathematical morphology based fault detection and faulty phase identification technique. Section 5 describes about simulation results and discussions. Conclusion of the proposed research work is discussed in section 6.

2. DOUBLE CIRCUIT TRANSMISSION LINE

The single line diagram of double circuit transmission line under study is depicted in Fig.1, which is used to check the performance of proposed mathematical morphological based fault detector. The proposed power system consists of a 400 kV, 50 Hz double circuit transmission line of 200 km length, connected to a 400 kV source at the sending and receiving end. Three phase current of both circuits of a double circuit transmission line is obtained from the location of the relay and processed using mathematical morphological filter. The model of double circuit transmission line is simulated for different types of shunt faults using Simscape Power System toolbox of Matlab.

Fig.1. Proposed test system

3. MATHEMATICAL MORPHOLOGY

Mathematical morphology (MM) is the time domain approach which can be used for the detection, classification and location of faults in the transmission line having attractive features like accuracy and simplicity. MM consists of two operations named as dilation (*dil*) and erosion (*erd*). Structuring Element (SE) is the basic function of morphological filtering. List of symbols and abbreviations are given below:

$A_1, B_1, C_1, A_2, B_2,$ *and* C_2	-	Phases of double circuit transmission line.
g	-	Ground.
Dil	-	Dilation.
Erd	-	Erosion.
Grad1	-	Gradient 1.
Grad2	-	Gradient 2.
Grad3	-	Gradient 3.
Grad1_f	-	Frequency of Gradient 1.
Grad2_f	-	Frequency of Gradient 2.
Grad3_f	-	Frequency of Gradient 3.
FL	-	Location of fault from bus 1 in kilometer.
R_f	-	Fault resistance in Ω.
R_g	-	Ground Resistance in Ω.
FIT	-	Fault inception time in seconds.

If $f(p)$ is the signal then its domain $D_f = \{x_0, x_1,\ldots,x_p\}$ and $s(q)$ is the structuring element having domain $D_q = \{y_1, y_2,\ldots,y_q\}$ and $p > q$, p and q are the integers, then the dilation of $f(p)$ by $s(q)$, denoted by $(f\oplus s)$ can be defined as:

$$y_d(p) = (f\oplus s)(p) = \max\{f(p-q)+s(q),\ 0\leq(p-q)\leq p,\ q\geq 0\} \quad (1)$$

The erosion of $f(p)$ by $s(q)$ denoted as $(f\ominus s)$ can be defined as:

$$y_e(p) = (f\ominus s)(p) = \min\{f(p+q)-s(q),\ 0\leq(p+q)\leq p,\ q\geq 0\} \quad (2)$$

The two operations named as opening and closing is defined as based on the dilation and erosion. The opening of $f(p)$ by $s(q)$, denoted as $(f\circ s)$ can be defined as dilation of the eroded signal by s:

$$y_o(p) = (f\circ s)(p) = (y_e\oplus s)(\pi)=((\Phi\ominus s)\oplus s)(\pi) \quad (3)$$

The closing of $f(p)$ by $s(q)$ denoted as $(f\cdot s)$ can be defined as erosion of the dilated signal $(f\oplus s)$ by s:

$$y_c(p) = (f\cdot s)(p)=(y_d\oplus s)(\pi)= ((\Phi\oplus s)\ominus s)(\pi) \quad (4)$$

4. PROPOSED TECHNIQUE

In the proposed work, mathematical morphological based fault detector has been introduced for the detection of double circuit transmission line faults. Proposed fault detection scheme is shown in Fig.2. Basic operations of mathematical morphology are defined as gradient-1 (grad1), gradient-2 (grad2) and gradient-3 (grad3). Detection of double circuit transmission line faults is completed by calculating the magnitudes of gradient-1, 2 and 3 of three phase fault current of circuit- 1 and 2.

Following the calculation of dilate and erode coefficients of three phase current of circuit-1 and 2, gradient-1 (also known as beucher gradient) is calculated by subtracting erode coefficient of three phase fault current from dilate coefficient of three phase fault current. Gradient-2 is calculated by subtracting erode coefficient of three phase fault current from three phase input fault current. Gradient-3 is calculated by subtracting three phase input fault current signal from dilate coefficient of three phase fault current. Furthermore, kurtosis of gradient-1, 2 and 3 are calculated separately.

Following the decomposition of three phase fault current of both circuits using mathematical morphology filter, the mathematical morphology based fault detector will declare the occurrence of fault on a double circuit transmission line when the magnitude of gradient-1, 2 or 3 of the faulted phase is found larger than the magnitude of gradient-1, 2 or 3 of an un-faulted phase. Proposed fault detector is tested for several types of faults. The main assistance of using proposed scheme is that it uses the fault data of three phase fault current measured at single end only for the protection of 100% transmission line length exclusive of fault current data of the other end [2].

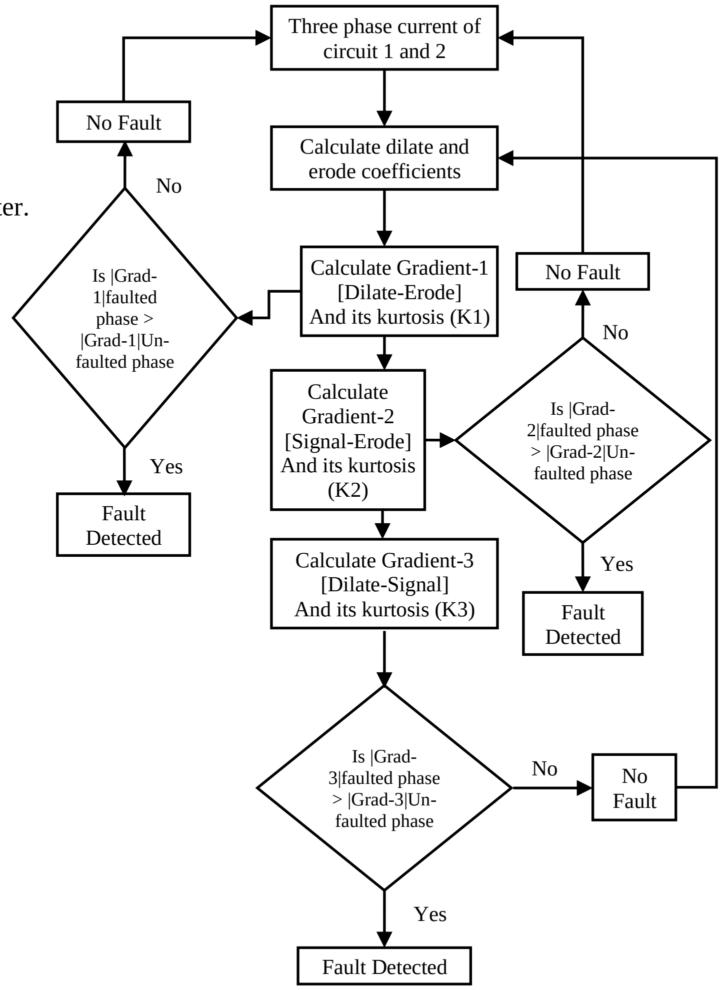

Fig.2. Proposed mathematical morphology based fault detection scheme

5. PERFORMANCE EVALUATION

To investigate the performance of the proposed fault detector, numerous shunt faults have been comprehensively tested. MATLAB has been used for achieving a variety of simulation studies. Simulation results of the proposed fault detector have been illustrated in the next subsections.

5.1 PERFORMANCE OF FAULT DETECTOR DURING NO-FAULT

By simulating the test system for no-fault, the performance of the proposed scheme is checked for healthy operation of a test system. The Fig.3 represents the three phase current of circuit-1 during no-fault. Similarly, three phase current of circuit-2 has been depicted in Fig.4. The gradients-1, 2 and 3 of phase-A1, B1 and C1 of circuit-1 and phase-A2, B2 and C2 of circuit-2 during no-fault have been shown in Fig.5-Fig.22. The performance of mathematical morphology based fault detector is examined for no-fault operation and the test results have been reported in Table.1. From Table.1, it is clear that the double circuit transmission line has no-fault.

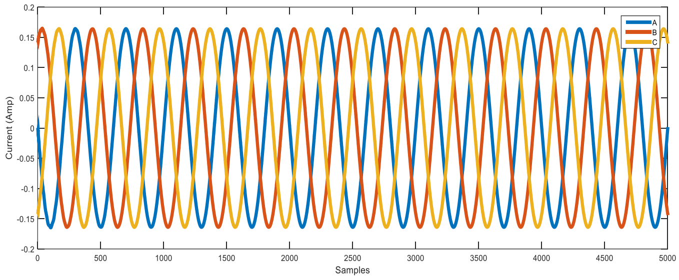

Fig.3. Three phase current of circuit-1 during no-fault

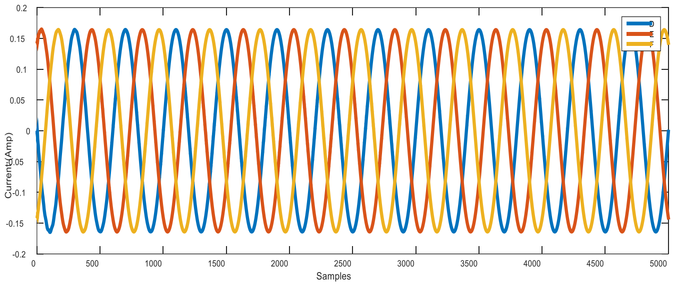

Fig.4. Three phase current of circuit-2 during no-fault

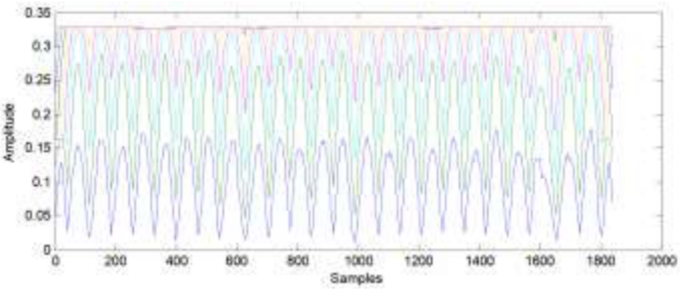

Fig.5. Gradient-1 of phase-A1 during no-fault

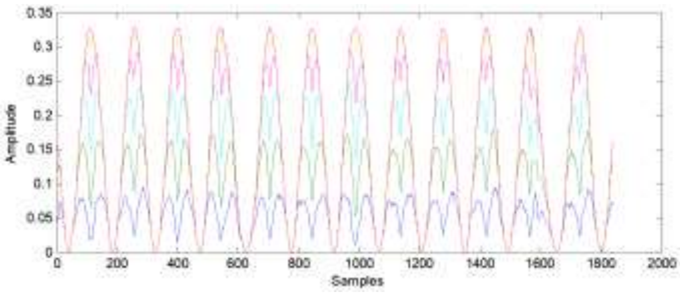

Fig.6. Gradient-2 of phase-A1 during no-fault

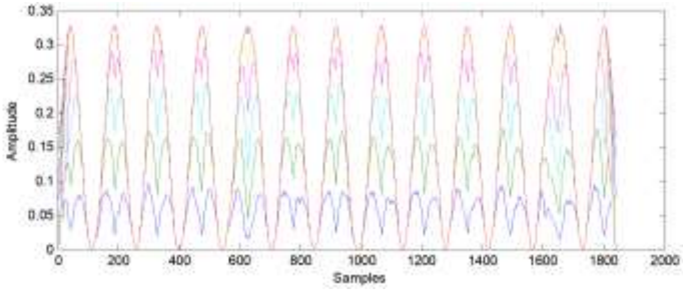

Fig.7. Gradient-3 of phase-A1 during no-fault

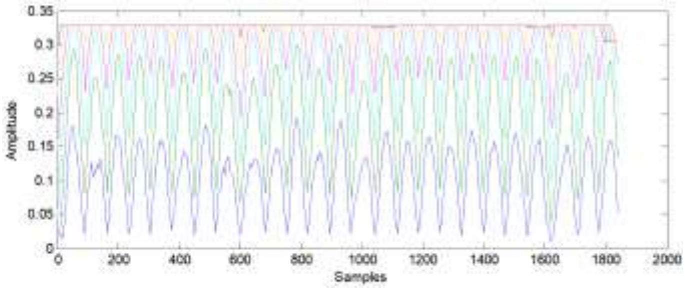

Fig.8. Gradient-1 of phase-B1 during no-fault

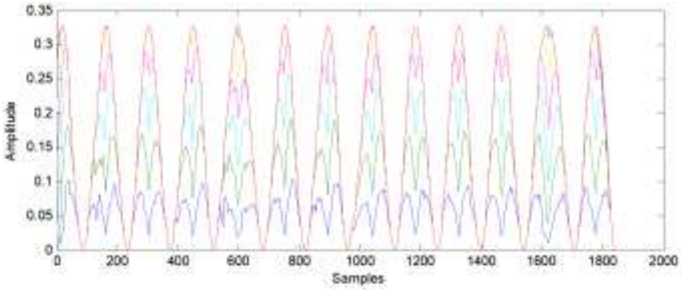

Fig.9. Gradient-2 of phase-B1 during no-fault

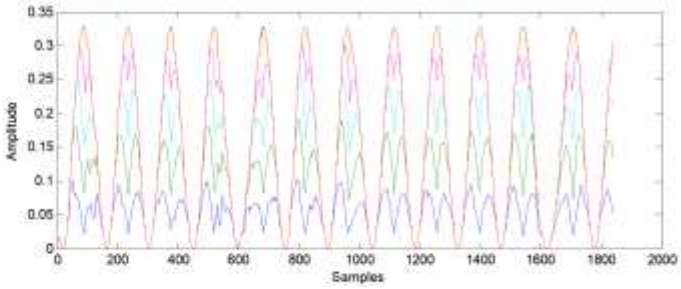

Fig.10. Gradient-3 of phase-B1 during no-fault

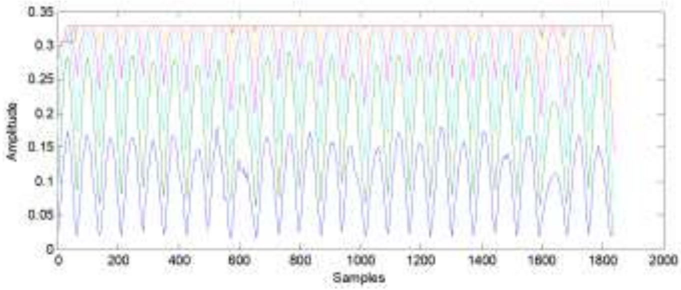

Fig.11. Gradient-1 of phase-C1 during no-fault

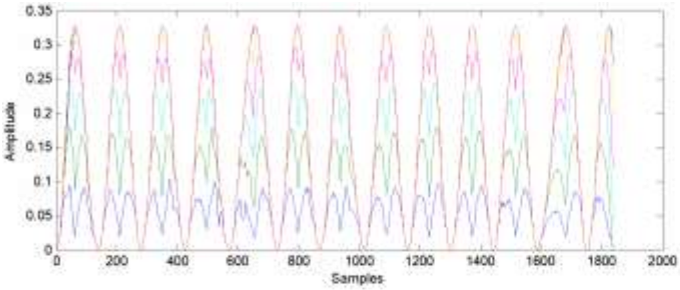

Fig.12. Gradient-2 of phase-C1 during no-fault

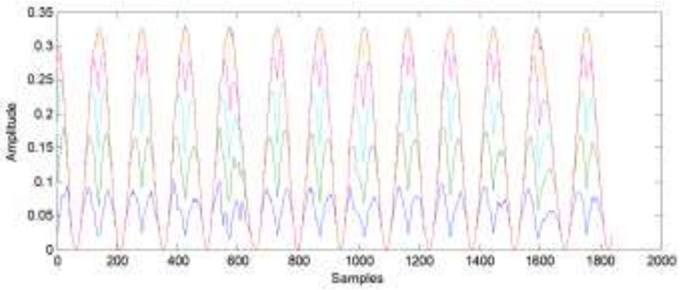

Fig.13. Gradient-3 of phase-C1 during no-fault

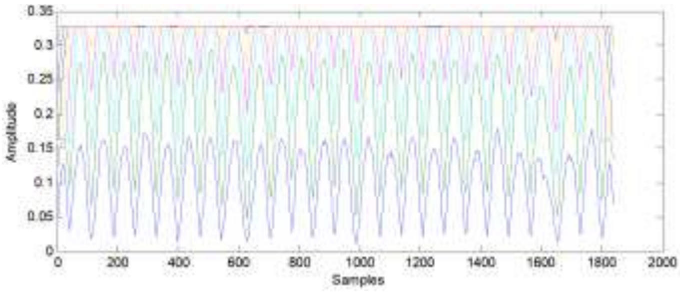

Fig.14. Gradient-1 of phase-A2 during no-fault

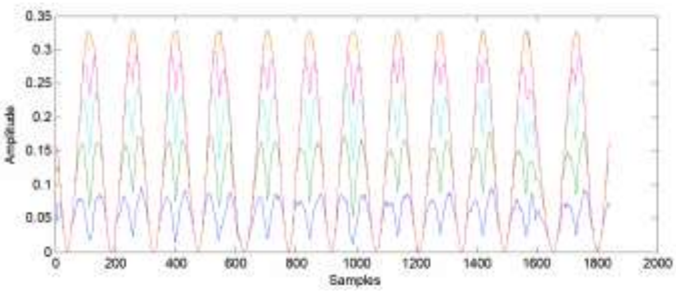

Fig.15. Gradient-2 of phase-A2 during no-fault

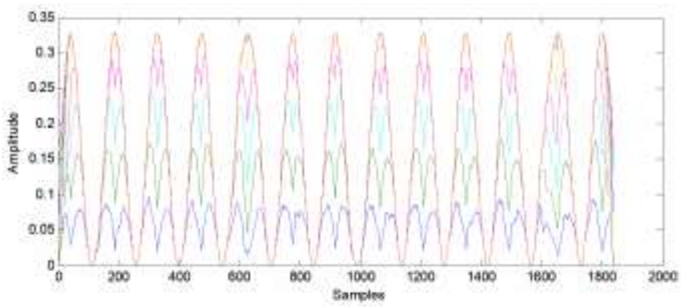

Fig.16. Gradient-3 of phase-A2 during no-fault

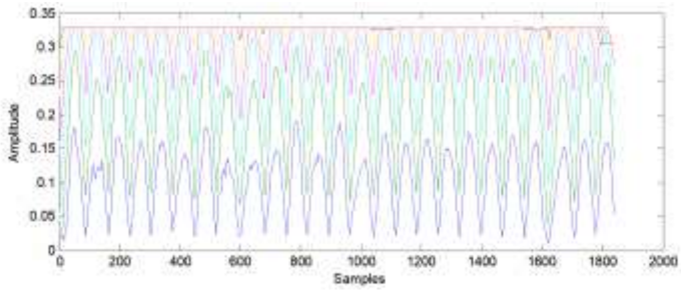

Fig.17. Gradient-1 of phase-B2 during no-fault

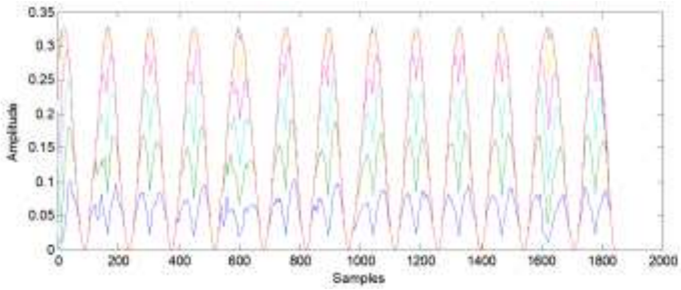

Fig.18. Gradient-2 of phase-B2 during no-fault

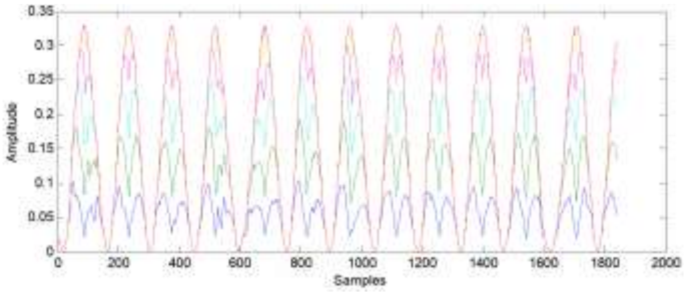

Fig.19. Gradient-3 of phase-B2 during no-fault

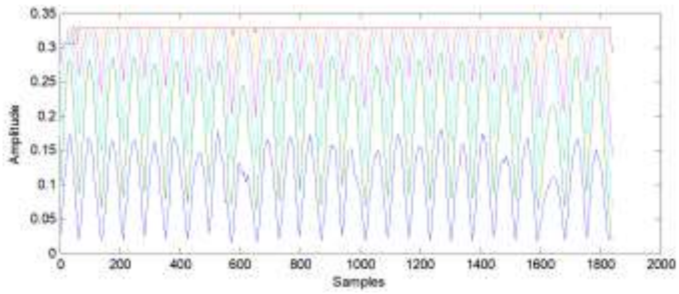

Fig.20. Gradient-1 of phase-C2 during no-fault

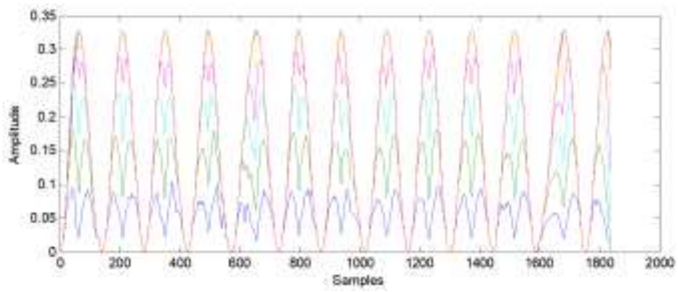

Fig.21. Gradient-2 of phase-C2 during no-fault

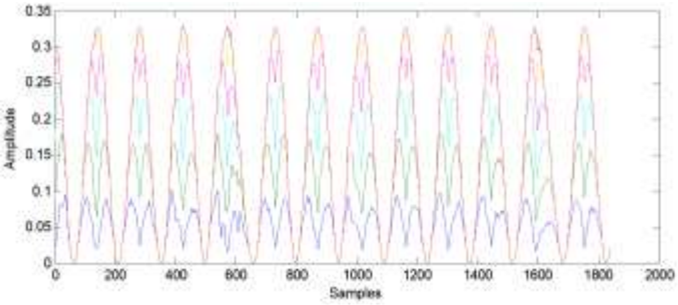

Fig.22. Gradient-3 of phase-C2 during no-fault

Table.1. Fault Detector Output for No-Fault

	Phase					
Output	**A1**	**B1**	**C1**	**A2**	**B2**	**C2**
Dil	0.1643	0.1640	0.1640	0.1643	0.1640	0.1640
Erd	0.1524	0.1543	0.1474	0.1524	0.1543	0.1474
Grad1	0.3282	0.3279	0.3280	0.3282	0.3279	0.3280
Grad2	0.3282	0.3279	0.3280	0.3282	0.3279	0.3280
Grad3	0.3282	0.3279	0.3280	0.3282	0.3279	0.3280

5.2 PERFORMANCE OF FAULT DETECTOR DURING SINGLE LINE TO GROUND FAULT

The performance of the fault detector is tested for phase-‘A1-g’ fault occurring at 100 km from bus-1 with fault inception time of 0.0166 seconds and $R_f = R_g = 0.001\Omega$. The three phase current of circuit-1 during phase-‘A1-g’ fault is shown in Fig.23. The Fig.24 depicts the three phase current of circuit-2 during phase-‘A1-g’ fault. The gradients-1, 2 and 3 of phase-A1, B1 and C1 of circuit-1 and phase-A2, B2 and C2 of circuit-2 during phase-‘A1-g’ fault have been shown in Fig.25-Fig.42. The Table.2 reports the response of the proposed fault detector for phase-‘A1-g’ fault occurring at 100 km from bus-1. As viewed from Table.2, the magnitude of gradient-1, 2 and 3 of faulted phase-A1 is greater than the magnitude of gradient 1, 2 and 3 of other phases and this explains that the proposed mathematical morphological based fault detector in actual fact detects phase-‘A1-g’ fault occurred on double circuit transmission line.

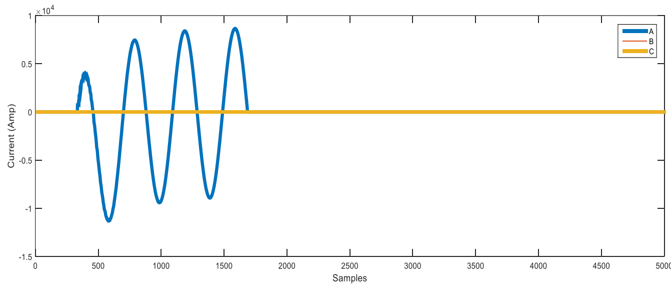

Fig.23. Three phase current of circuit-1 during phase- ‘A1-g’ fault

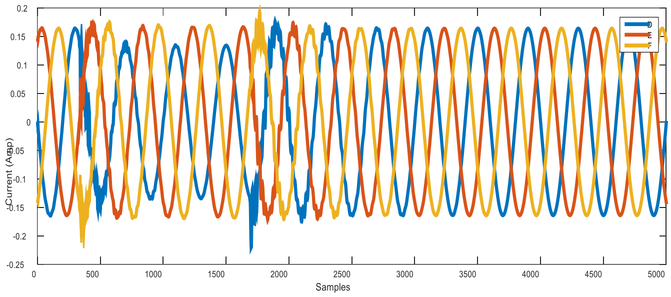

Fig.24. Three phase current of circuit-2 during phase- ‘A1-g’ fault

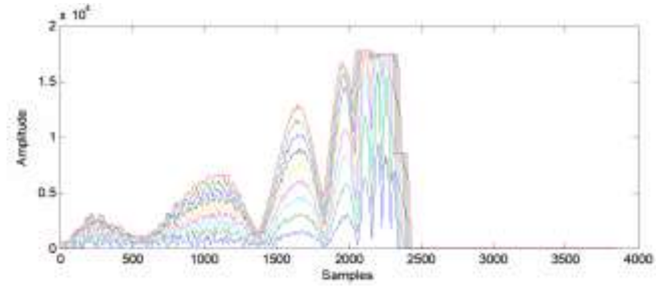

Fig.25. Gradient-1 of phase-A1 during phase-‘A1-g’ fault

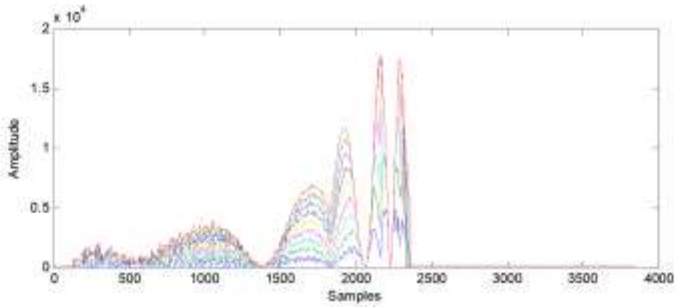

Fig.26. Gradient-2 of phase-A1 during phase-‘A1-g’ fault

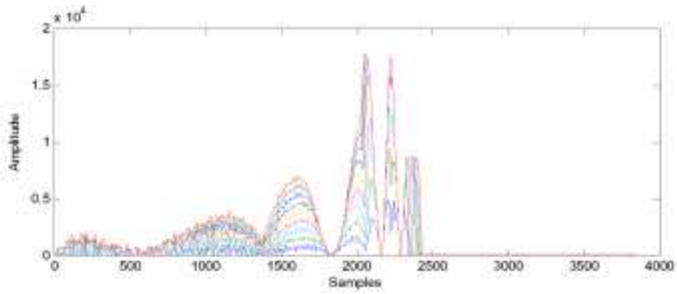

Fig.27. Gradient-3 of phase-A1 during phase-‘A1-g’ fault

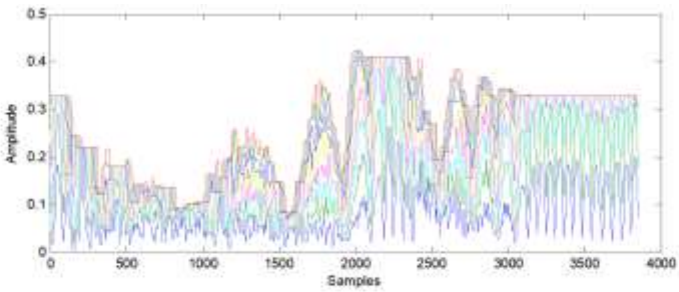

Fig.28. Gradient-1 of phase-B1 during phase-‘A1-g’ fault

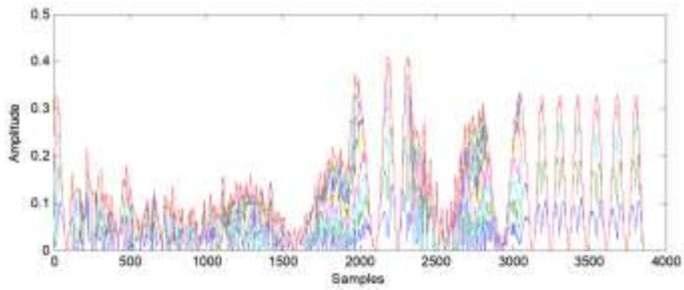

Fig.29. Gradient-2 of phase-B1 during phase-'A1-g' fault

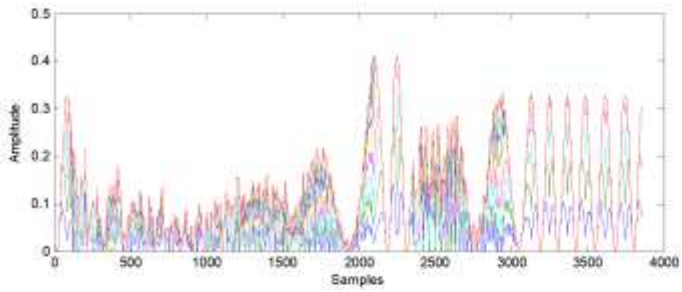

Fig.30. Gradient-3 of phase-B1 during phase-'A1-g' fault

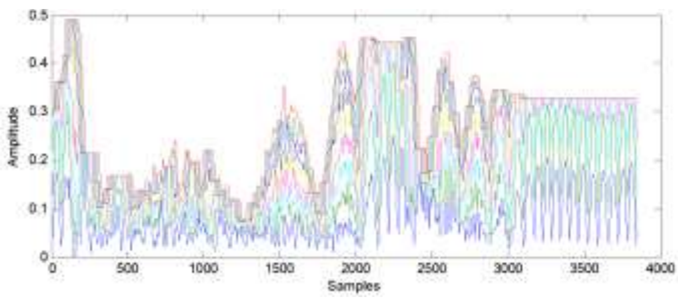

Fig.31. Gradient-1 of phase-C1 during phase-'A1-g' fault

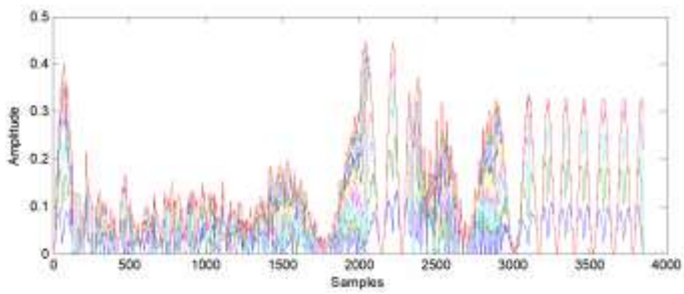

Fig.32. Gradient-2 of phase-C1 during phase-'A1-g' fault

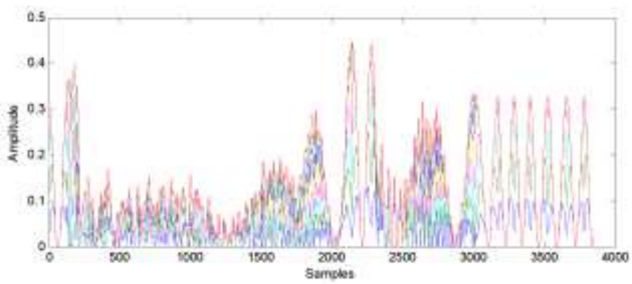

Fig.33. Gradient-3 of phase-C1 during phase-'A1-g' fault

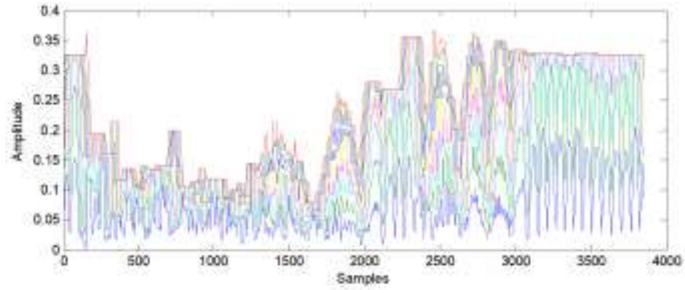

Fig.34. Gradient-1 of phase-A2 during phase-'A1-g' fault

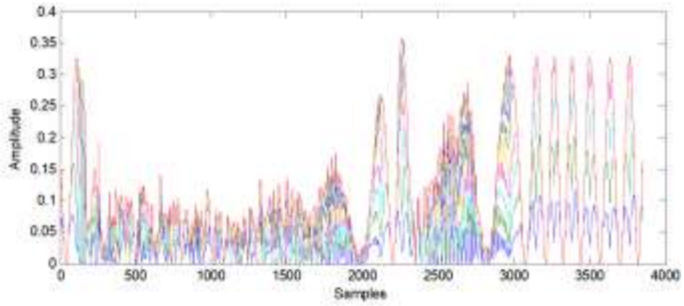

Fig.35. Gradient-2 of phase-A2 during phase-'A1-g' fault

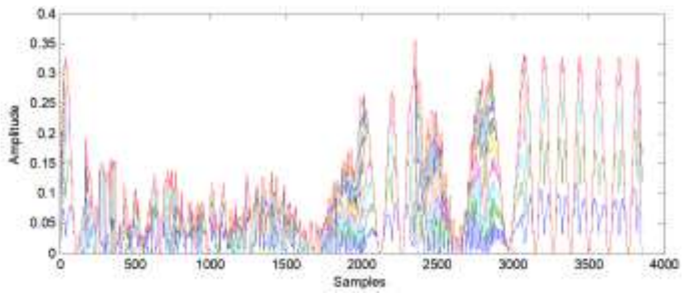

Fig.36. Gradient-3 of phase-A2 during phase-'A1-g' fault

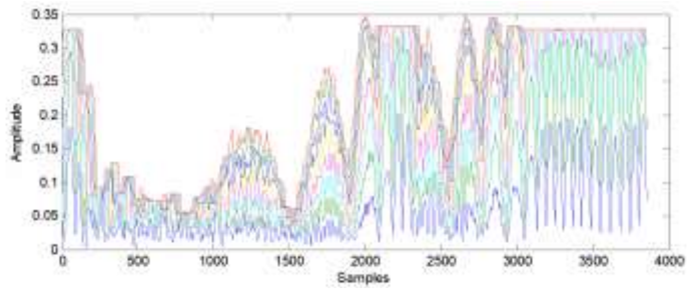

Fig.37. Gradient-1 of phase-B2 during phase-'A1-g' fault

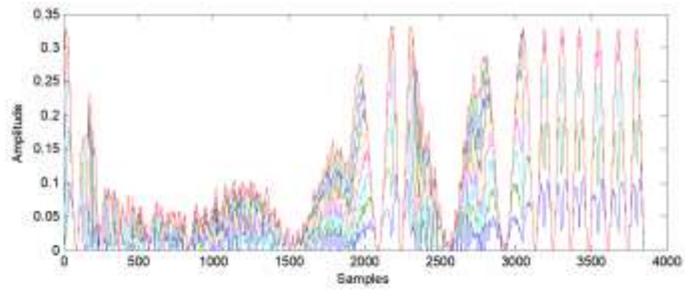

Fig.38. Gradient-2 of phase-B2 during phase-'A1-g' fault

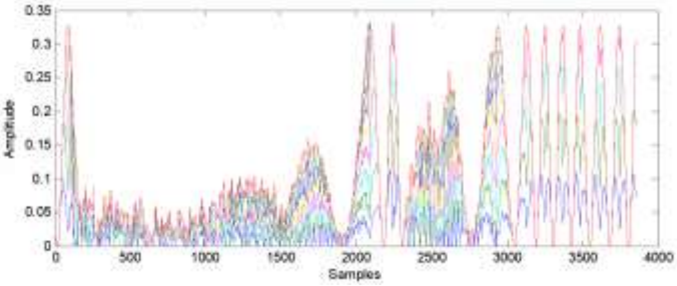

Fig.39. Gradient-3 of phase-B2 during phase-‘A1-g’ fault

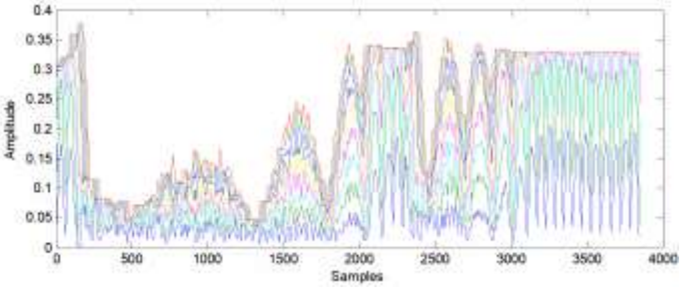

Fig.40. Gradient-1 of phase-C2 during phase-‘A1-g’ fault

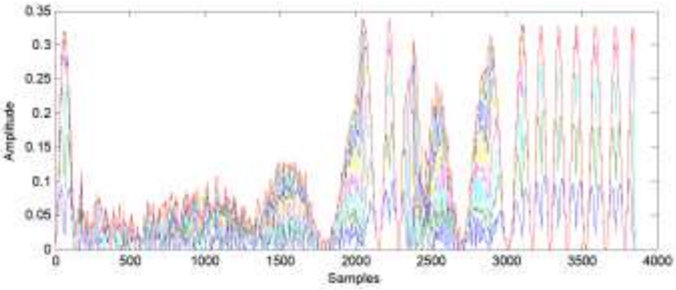

Fig.41. Gradient-2 of phase-C2 during phase-‘A1-g’ fault

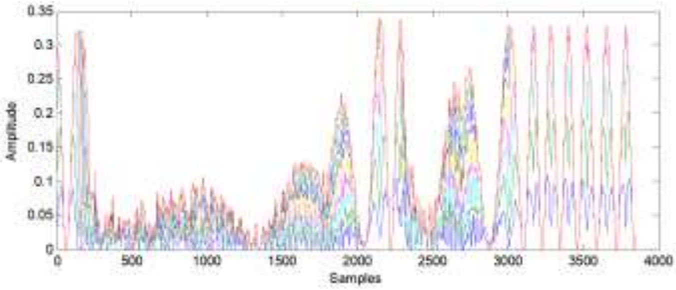

Fig.42. Gradient-3 of phase-C2 during phase-‘A1-g’ fault

Table.2. Fault Detector Output for Phase-‘A1-G’ Fault at F_{it} = 0.0166 Seconds with $R_F = R_G = 0.001\Omega$, F_L = 100 KM

	Phase					
Output	**A1**	**B1**	**C1**	**A2**	**B2**	**C2**
Dil	8.6440 $*10^3$	0.2552	0.2544	0.2028	0.1956	0.1944
Erd	7.4788 $*10^3$	0.2183	0.2251	0.1554	0.1667	0.1766
Grad1	1.7800 $*10^4$	0.4218	0.4897	0.3685	0.3483	0.3792
Grad1_f	1.5475 $*10^6$	425.633	363.631	353.037	317.335	190.932
Grad2	1.7800 $*10^4$	0.4123	0.4482	0.3569	0.3330	0.3410
Grad2_f	7.7491 $*10^5$	140.676	241.852	113.704	98.259	35.1962
Grad3	1.7800 $*10^4$	0.4123	0.4482	0.3569	0.3330	0.3410
Grad3_f	7.7257 $*10^5$	52.446	87.1679	113.228	87.3264	58.788

5.3 PERFORMANCE OF FAULT DETECTOR DURING DOUBLE LINE TO GROUND FAULT

The performance of the fault detector is tested for phase-‘A1A2-g’ fault occurring at 100 km from bus-1 with fault inception time of 0.0166 seconds and $R_f = R_g = 0.001\Omega$. The three phase current of circuit-1 during phase-‘A1A2-g’ fault is shown in Fig.43. Fig.44 depicts the three phase current of circuit-2 during phase-‘A1A2-g’ fault. The gradients-1, 2 and 3 of phase-A1, B1 and C1 of circuit-1 and phase-A2, B2 and C2 of circuit-2 during phase-‘A1A2-g’ fault have been shown in Fig.45-Fig.62. The Table.3 reports the response of the proposed fault detector for phase-‘A1A2-g’ fault occurring at 100 km from bus-1. As viewed from Table.3, the magnitude of gradient-1, 2 and 3 of faulted phase-A1 and A2 is greater than the magnitude of gradient 1, 2 and 3 of un-faulted phases and this explains that the proposed fault detector in actual fact detects phase-‘A1A2-g’ fault occurred on double circuit transmission line.

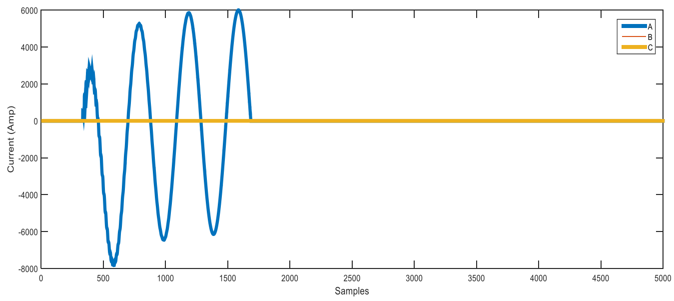

Fig.43. Three phase current of circuit-1 during ‘A1A2-g’ fault

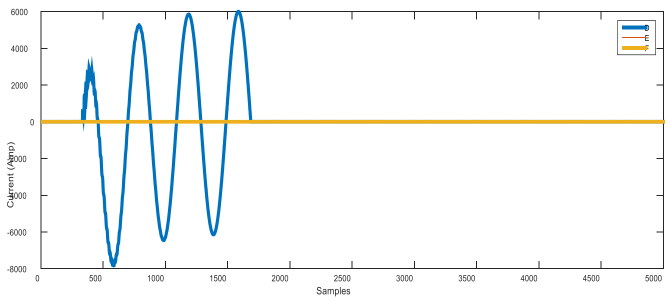

Fig.44. Three phase current of circuit-2 during ‘A1A2-g’ fault

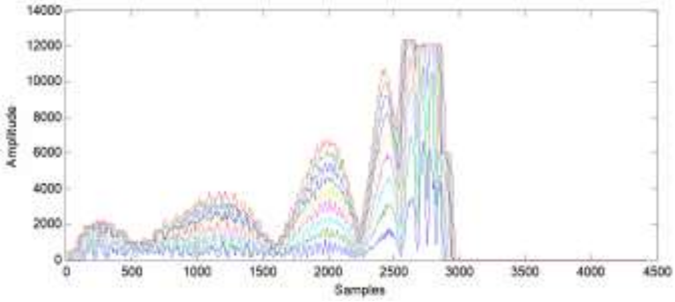

Fig.45. Gradient-1 of phase-A1 during phase-‘A1A2-g’ fault

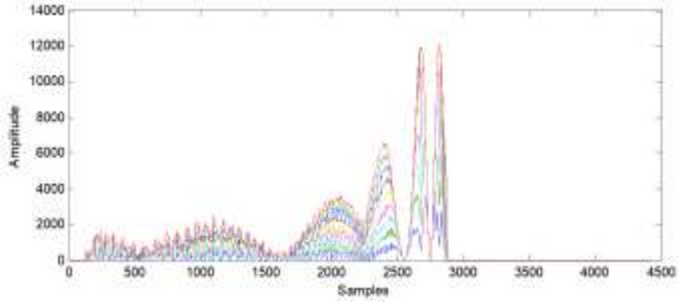

Fig.46. Gradient-2 of phase-A1 during phase-‘A1A2-g’ fault

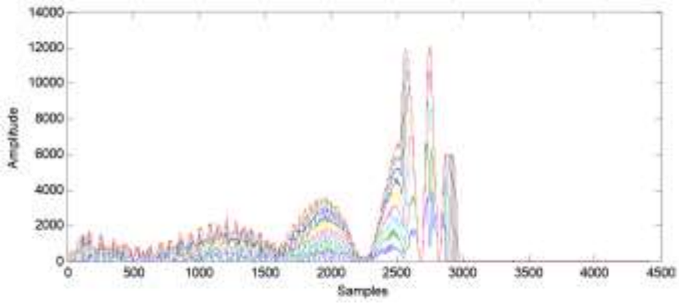

Fig.47. Gradient-3 of phase-A1 during phase-‘A1A2-g’ fault

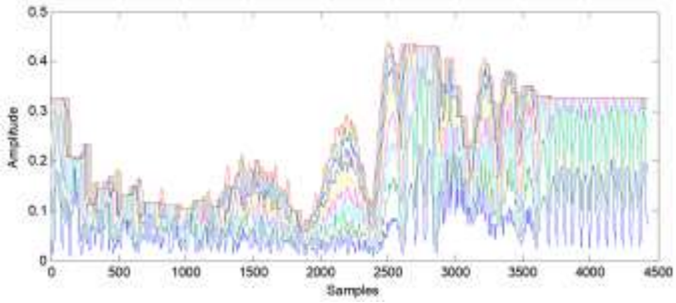

Fig.48. Gradient-1 of phase-B1 during phase-‘A1A2-g’ fault

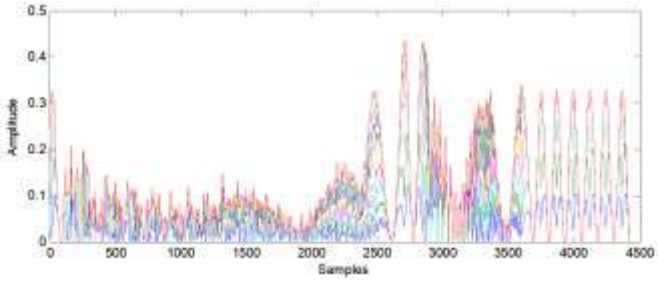

Fig.49. Gradient-2 of phase-B1 during phase-‘A1A2-g’ fault

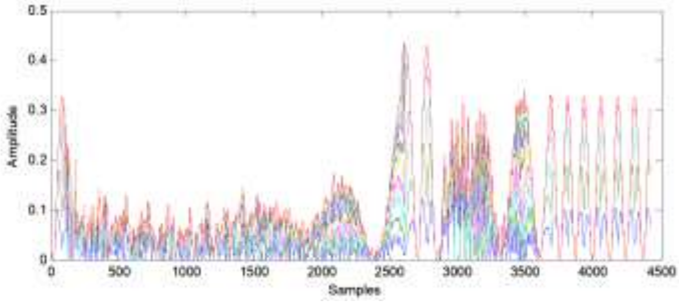

Fig.50. Gradient-3 of phase-B1 during phase-‘A1A2-g’ fault

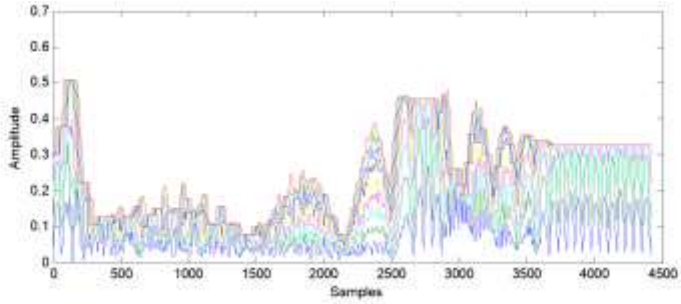

Fig.51. Gradient-1 of phase-C1 during phase-‘A1A2-g’ fault

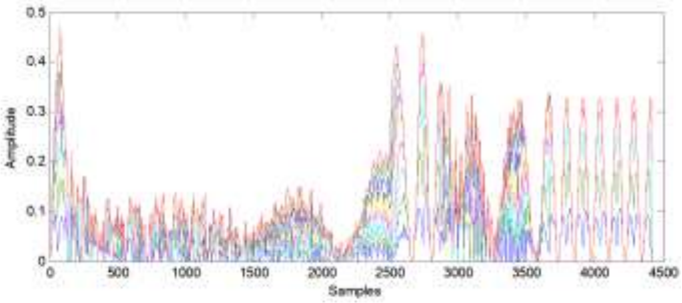

Fig.52. Gradient-2 of phase-C1 during phase-‘A1A2-g’ fault

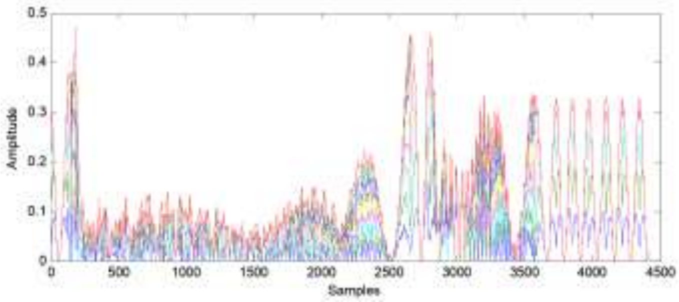

Fig.53. Gradient-3 of phase-C1 during phase-‘A1A2-g’ fault

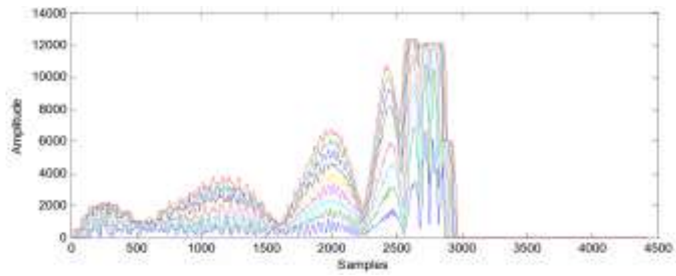

Fig.54. Gradient-1 of phase-A2 during phase-‘A1A2-g’ fault

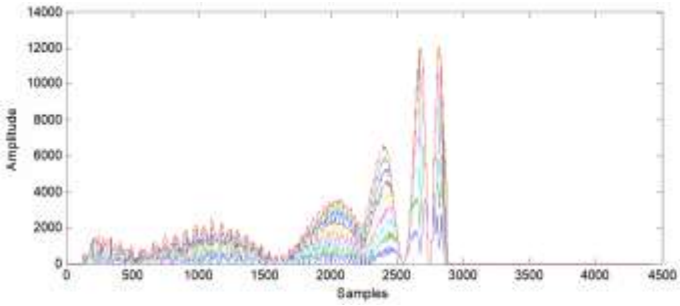

Fig.55. Gradient-2 of phase-A2 during phase-‘A1A2-g’ fault

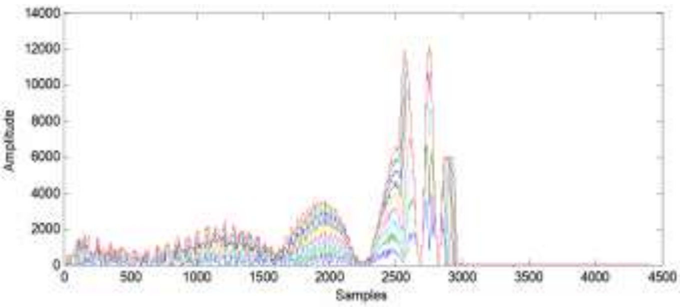

Fig.56. Gradient-3 of phase-A2 during phase-‘A1A2-g’ fault

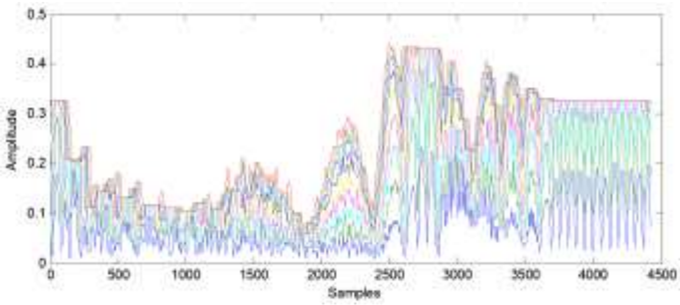

Fig.57. Gradient-1 of phase-B2 during phase-‘A1A2-g’ fault

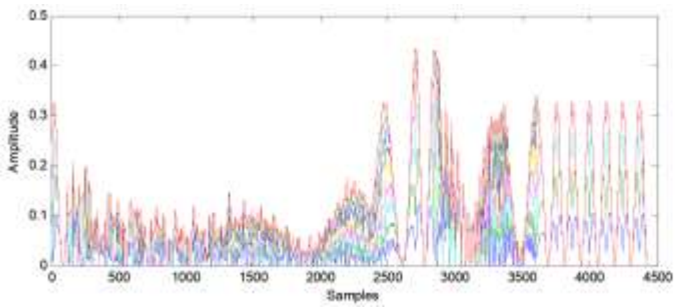

Fig.58. Gradient-2 of phase-B2 during phase-‘A1A2-g’ fault

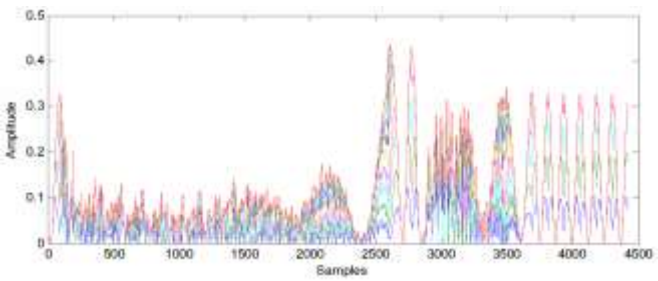

Fig.59. Gradient-3 of phase-B2 during phase-‘A1A2-g’ fault

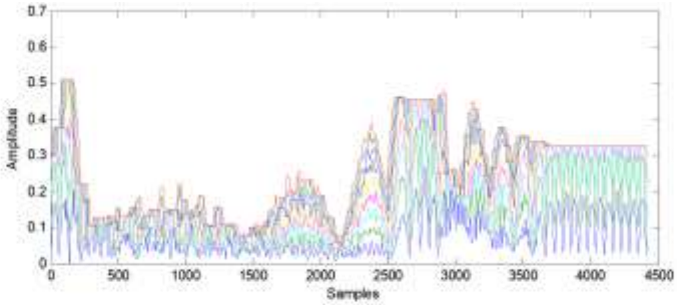

Fig.60. Gradient-1 of phase-C2 during phase-‘A1A2-g’ fault

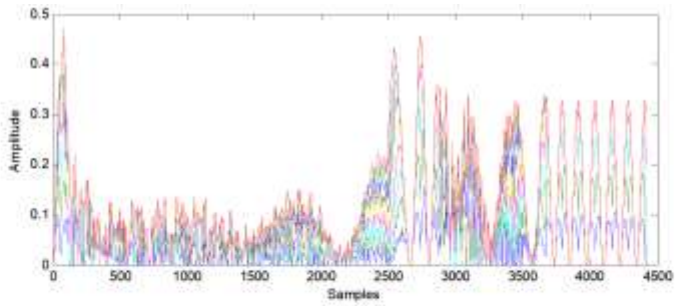

Fig.61. Gradient-2 of phase-C2 during phase-‘A1A2-g’ fault

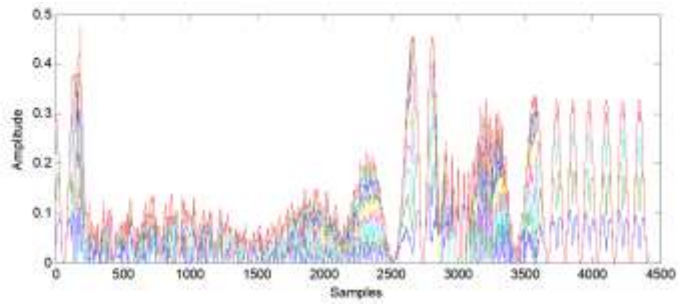

Fig.62. Gradient-3 of phase-C2 during phase-‘A1A2-g’ fault

Table.3. Fault Detector Output for Phase-‘A1A2-G’ Fault at F_{it} = 0.0166 Sec, $R_F = R_G = 0.001\Omega$ AND F_L = 100 KM

	Phase					
Output	**A1**	**B1**	**C1**	**A2**	**B2**	**C2**
Dil	$5.9963*10^3$	0.2689	0.2630	$5.9963*10^3$	0.2689	0.2730
Erd	$5.3653*10^3$	0.2270	0.2343	$5.3653*10^3$	0.2270	0.2343
Grad1	$1.2335*10^4$	0.4414	0.5098	$1.2335*10^4$	0.4414	0.5098
Grad1_f	$9.3573*10^5$	325.550	266.491	$9.3573*10^5$	325.551	266.490
Grad2	$1.2136*10^4$	0.4344	0.4724	$1.2136*10^4$	0.4344	0.4724
Grad2_f	$4.6860*10^5$	109.236	149.617	$4.6860*10^5$	109.236	149.617
Grad3	$1.2136*10^4$	0.4344	0.4724	$1.2136*10^4$	0.4344	0.4724

Grad3_f	4.6714 $*10^5$	106.686	80.2134	4.6714 $*10^5$	106.686	80.213

5.4 PERFORMANCE DURING TRIPLE LINE TO GROUND FAULT

The performance of the fault detector is checked for phase-'B1B2C2-g' fault occurring at 100 km from bus-1 with fault inception time of 0.0166 seconds and $R_f = R_g = 0.001\Omega$. The three phase current of circuit-1 during phase-'B1B2C2-g' fault is shown in Fig.63. The Fig.64 depicts the three phase current of circuit-2 during phase-'B1B2C2-g' fault. The gradients-1, 2 and 3 of phase-A1, B1 and C1 of circuit-1 and phase-A2, B2 and C2 of circuit-2 during phase-'B1B2C2-g' fault have been shown in Fig.65 - Fig.82. The Table.4 reports the response of the proposed fault detector for phase-'B1B2C2-g' fault occurring at 100 km from bus-1. As viewed from Table.4, the magnitude of gradient-1, 2 and 3 of faulted phase-B1, B2 and C2 is greater than the magnitude of gradient 1, 2 and 3 of un-faulted phases and this explains that the proposed mathematical morphological based fault detector in actual fact detects phase-'B1B2C2-g' fault occurred at 100 km from bus-1 on double circuit transmission line.

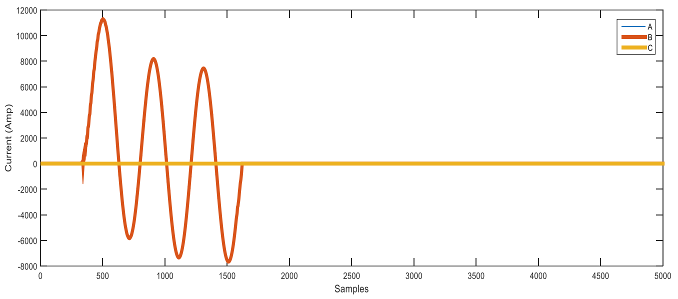

Fig.63. Three phase current of circuit-1 during 'B1B2C2-g' fault

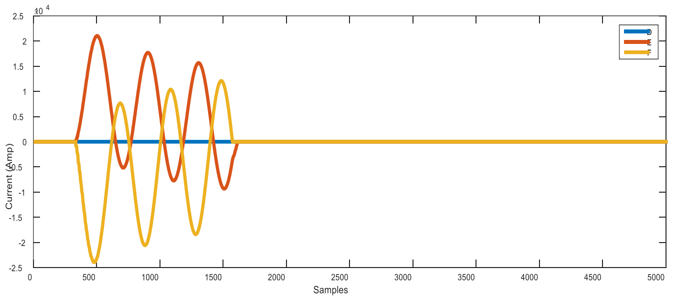

Fig.64. Three phase current of circuit-2 during 'B1B2C2-g' fault

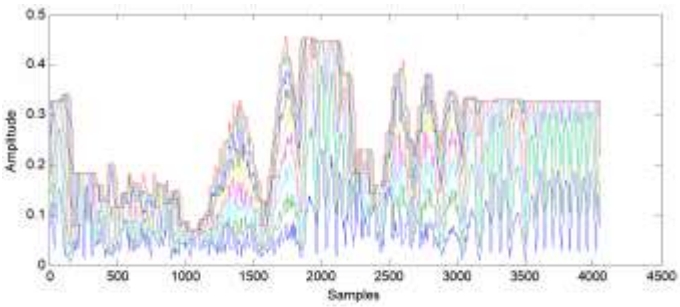

Fig.65. Gradient-1 of phase-A1 during phase-'B1B2C2-g' fault

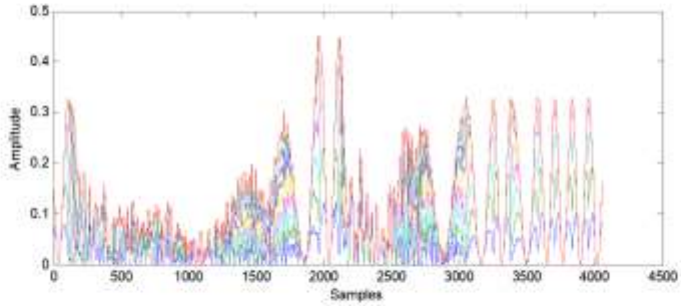

Fig.66. Gradient-2 of phase-A1 during phase-'B1B2C2-g' fault

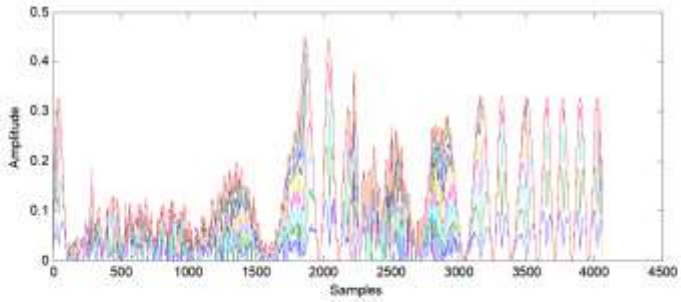

Fig.67. Gradient-3 of phase-A1 during phase-'B1B2C2-g' fault

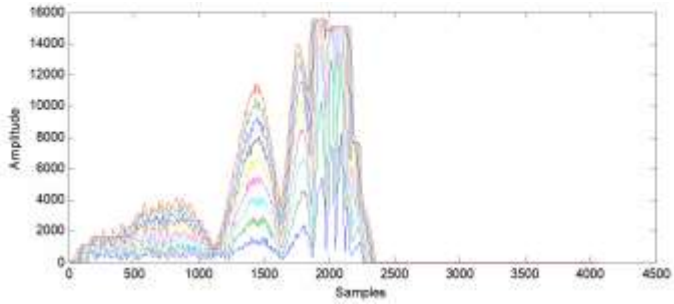

Fig.68. Gradient-1 of phase-B1 during phase-'B1B2C2-g' fault

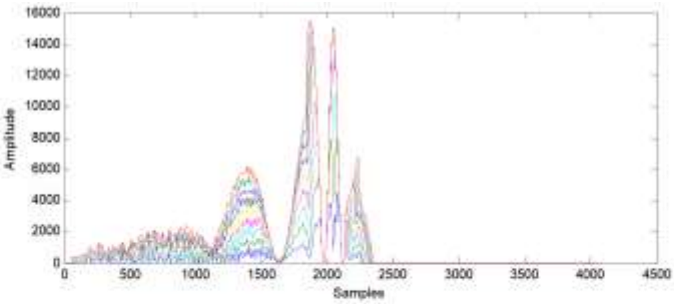

Fig.69. Gradient-2 of phase-B1 during phase-'B1B2C2-g' fault

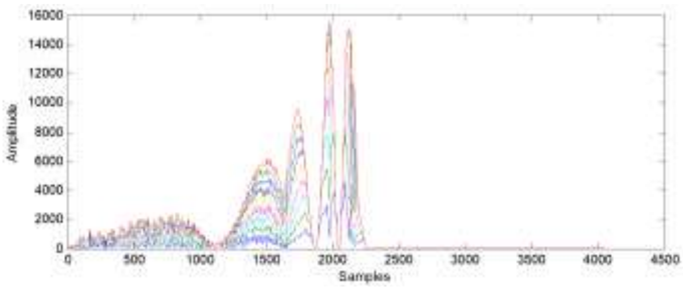

Fig.70. Gradient-3 of phase-B1 during phase-'B1B2C2-g' fault

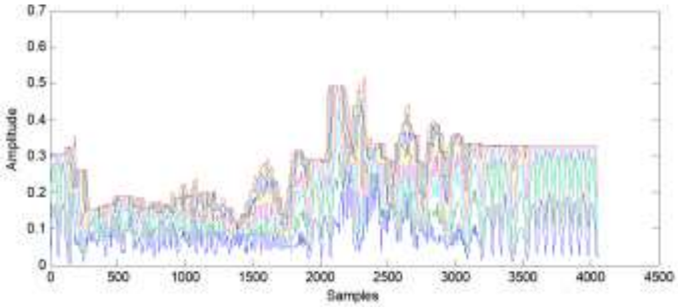

Fig.71. Gradient-1 of phase-C1 during phase-‘B1B2C2-g’ fault

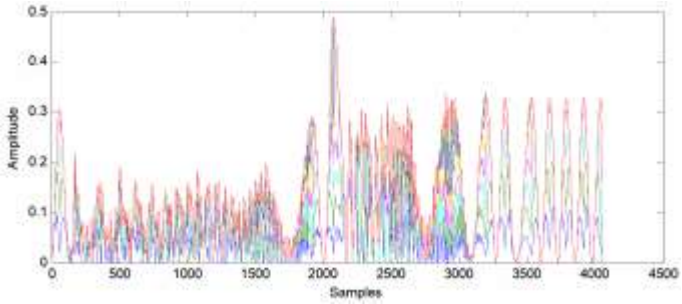

Fig.72. Gradient-2 of phase-C1 during phase-‘B1B2C2-g’ fault

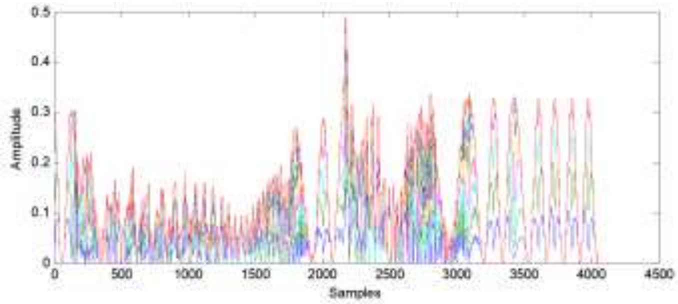

Fig.73. Gradient-3 of phase-C1 during phase-‘B1B2C2-g’ fault

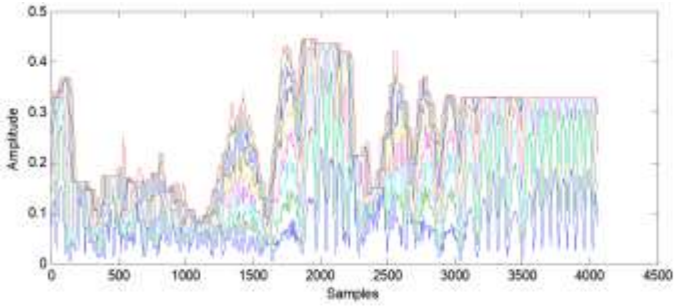

Fig.74. Gradient-1 of phase-A2 during phase-‘B1B2C2-g’ fault

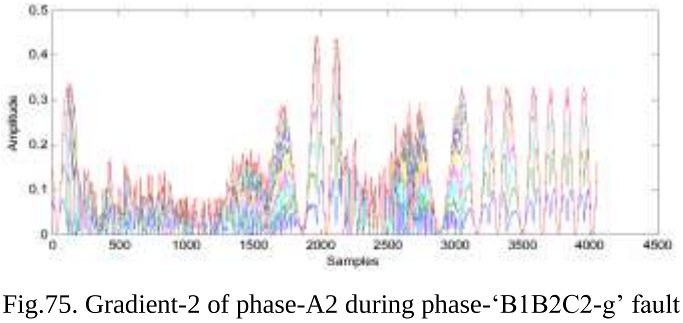

Fig.75. Gradient-2 of phase-A2 during phase-‘B1B2C2-g’ fault

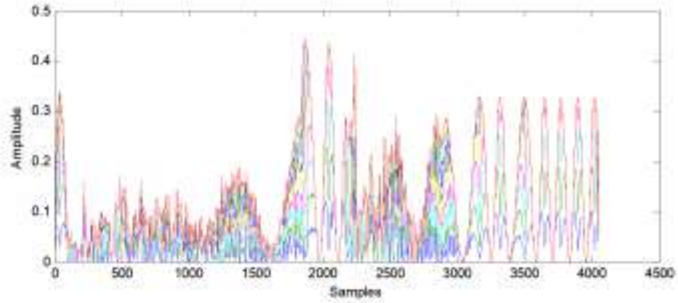

Fig.76. Gradient-3 of phase-A2 during phase-‘B1B2C2-g’ fault

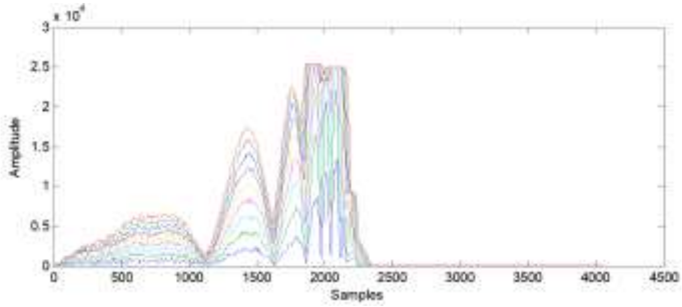

Fig.77. Gradient-1 of phase-B2 during phase-‘B1B2C2-g’ fault

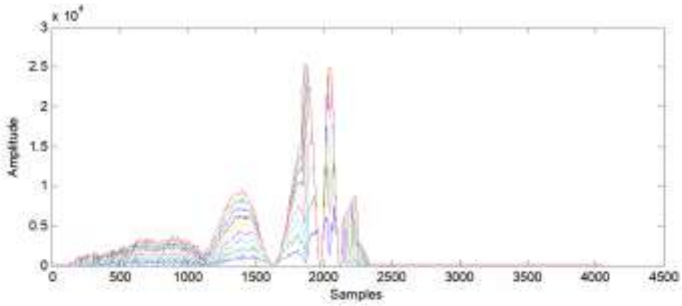

Fig.78. Gradient-2 of phase-B2 during phase-‘B1B2C2-g’ fault

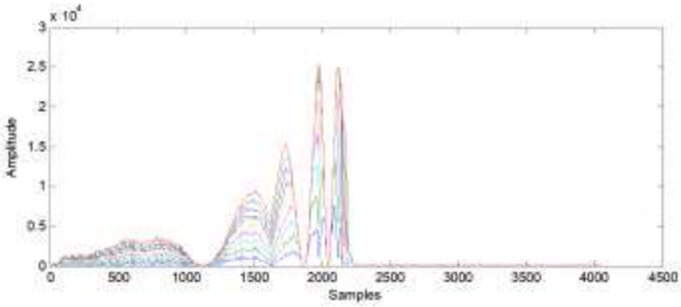

Fig.79. Gradient-3 of phase-B2 during phase-‘B1B2C2-g’ fault

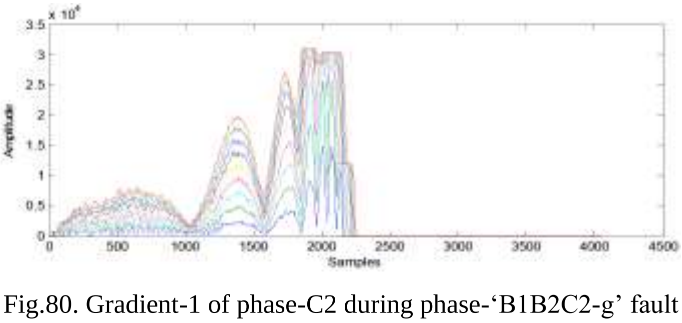

Fig.80. Gradient-1 of phase-C2 during phase-‘B1B2C2-g’ fault

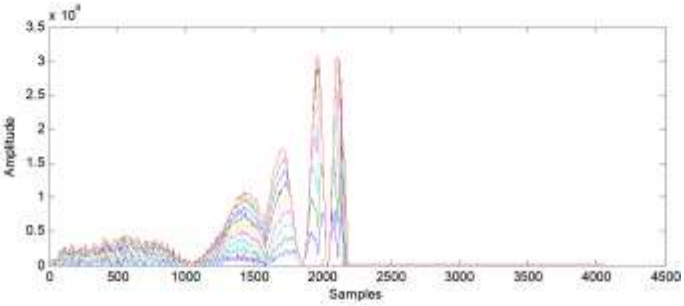

Fig.81. Gradient-2 of phase-C2 during phase-‘B1B2C2-g’ fault

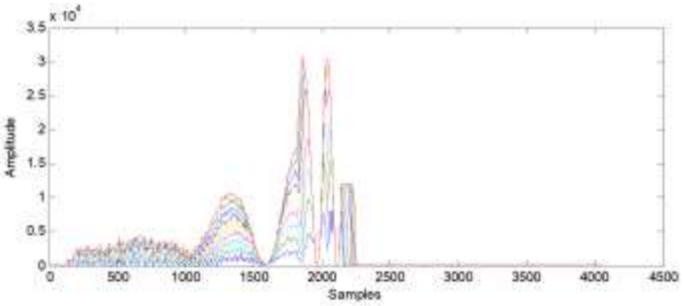

Fig.82. Gradient-3 of phase-C2 during phase-‘B1B2C2-g’ fault

Table.4. Fault Detector Output for Phase-‘B1B2C2-G’ Fault at F_{it} = 0.0166 Sec. $R_F = R_G = 0.001\Omega$, F_L = 100 KM

	Phase					
Output	**A1**	**B1**	**C1**	**A2**	**B2**	**C2**
Dil	0.2379	1.1478* 10^4	0.2400	0.2403	2.1083 *10^4	1.2040 *10^4
Erd	0.2071	1.1209* 10^4	0.1532	0.2033	2.0930 *10^4	1.0894 *10^4
Grad1	0.4581	1.5525* 10^4	0.5153	0.4465	2.5397 *10^4	3.0966 *10^4
Grad1_f	449.161	3.6171* 10^6	382.039	422.963	2.7606 *10^6	3.5241 *10^6
Grad2	0.4518	1.5525* 10^4	0.4907	0.4465	2.5392 *10^4	3.0770 *10^4
Grad2_f	147.571	1.8171* 10^6	71.484	155.177	1.3861 *10^6	1.7473 *10^6
Grad3	0.4518	1.5525* 10^4	0.4907	0.4465	2.5392 *10^4	3.0770 *10^4
Grad3_f	146.300	9.4672* 10^5	145.394	147.804	1.3745 *10^6	1.7768 *10^6

6. CONCLUSION

Mathematical morphology based fault detector for double circuit transmission line has been established to be very useful beneath different fault circumstances. Three phase fault current of both circuits of a double circuit transmission line is processed using mathematical morphological filter. The proposed fault detector uses only single end fault current samples. The consistency of the proposed fault detector is not affected by fault type variation. The simulation results show that mathematical morphology based fault detector accurately detects the fault and identifies the faulty phase.

REFERENCES

[1] P.N. Gawande and S.S. Dambhare, “Enhancing Security of Distance Relays during Power Swing Unblocking Function for Double Circuit Transmission Lines: A Differential Power Approach”, *Proceedings of 13th IET International Conference on Development in Power System Protection*, pp. 1-6, 2016.

[2] A. Swetapadma and A. Yadav, “Protection of Parallel Transmission Lines including Inter-Circuit Faults using Naïve Bayes Classifier”, *Alexandria Engineering Journal*, Vol. 55, No. 2, pp. 1411-1419, 2016.

[3] N. Kang, J. Chen and Y. Liao, “A Fault-Location Algorithm for Series-Compensated Double-Circuit Transmission Lines Using the Distributed Parameter Line Model”, *IEEE Transactions on Power Delivery*, Vol. 30, No. 1, pp. 360-367, 2015.

[4] A. Swetapadma and A. Yadav, “Time Domain Complete Protection Scheme for Parallel Transmission Lines”, *Ain Shams Engineering Journal*, Vol. 7, No. 1, pp. 169-183, 2015.

[5] M.B. Hessine, H. Jouini and S, Chebbi, “Fault Detection and Classification Approaches in Transmission Lines using Artificial Neural Networks”. *Proceedings of 17th IEEE Mediterranean Electrotechnical Conference*, pp. 515-519, 2014.

[6] S.M. Hashemi, M.T. Hagh and H. Seyedi, “A Novel Backup Distance Protection Scheme for Series Compensated Transmission Lines”, *IEEE Transactions on Power Delivery*, Vol. 29, No. 2, pp. 699-707, 2014.

[7] M.M. Saha, P. Balcerek, P. Pierz, E. Rosolowski and J. Izykowski, “New and Fast Method of Determining the Faulted Circuit in the Parallel Lines with use of One-end Current Measurements”, *Proceedings of 12th IET International Conference on Developments in Power System Protection*, pp. 1-6, 2014.

[8] N. Perera and A.D. Rajapakse, “Series-Compensated Double-Circuit Transmission-Line Protection using Directions of Current Transients”, *IEEE Transactions on Power Delivery*, Vol. 28, No. 3, pp. 1566-1575, 2013.

[9] R. Kumar, A. Sinha and G.K. Choudhary, “A New Digital Distance Relaying Algorithm for First Zone Protection for Series Compensated Double Circuit Transmission Lines”, *Proceedings of 3rd International Conference on Advances in Computing and Communications*, pp. 102-106, 2013.

[10] M.R. Noori and S.M. Shahrtash, “A Novel Faulted Phase Selector for Double Circuit Transmission Lines by Employing Adaptive Cumulative Sum-Based Method”, *Proceedings of 11th International Conference on Environment and Electrical Engineering*, pp. 365-370, 2012.

[11] E. Koley, A. Yadav, A.S. Thoke, A. Jain and S. Ghosh, “Detection and Classification of Faults on Six Phase Transmission Line using ANN”, *Proceedings of 2nd International Conference on Computer and Communication Technology*, pp. 100-103, 2011.

[12] Y. Wang, Wang, Y., D. Zhou, Y.J. Jiao and S.X. Xu, “Fault Location and Phase Selection for UHV Six Phase Transmission Lines”, *Proceedings of Power and Energy Engineering Conference*, pp. 1-7, 2011.

[13] M.A. Golkar, R. Shariatinasa and M. Akbari, "Voltage Stability Analysis in Conversion of Double Three Phase to Six Phase Transmission Line", *Proceedings of IEEE International Conference on Power and Energy*, pp. 172-177, 2011.
[14] A. Hosny and M. Safiuddin, "ANN Based Protection System for Controllable Series Compensated Transmission Lines", *Proceedings of IEEE Power Systems Conference and Exposition*, pp. 172-177, 2009.
[15] V.J. Pandya and S.A. Kanitkar, "A Novel Unit Protection Scheme for Protection of Series Compensated Transmission Line Using Wavelet Transform", *Proceedings of IEEE Power Engineering Conference*, pp. 1-5, 2007.